COVER SHEET

A vibrational spectroscopic study of perhamite, an unusual silico-phosphate.

Ray L. Frost[Ψa] Matt L. Weier [a] and Stuart J. Mills [•b,c]

[a] Inorganic Materials Research Program, School of Physical and Chemical Sciences, Queensland University of Technology, GPO Box 2434, Brisbane, Queensland 4001, Australia.
[b] Geosciences, Museum Victoria, PO Box 666E, Melbourne, Victoria 3001, Australia.
[c] CSIRO Minerals, Box 312, Clayton South, Victoria 3169, Australia.

Abstract

The silico-phosphate mineral perhamite has been studied using a combination of electron and vibrational spectroscopy. SEM photomicrographs reveal that perhamite morphology consists of very thin intergrown platelets that can form a variety of habits. Infrared spectroscopy in the hydroxyl-stretching region shows a number of overlapping bands which are observed in the range 3581–3078 cm^{-1}. These wavenumbers enable an estimation to be made of the hydrogen bond distances in perhamite: 3.176(0), 2.880(5), 2.779(6), 2.749(3), 2.668(1) and 2.599(7) Å. Intense Raman bands are observed in the region 1110–1130 and 966–996 cm^{-1} and are assigned to the SiO_4 and PO_4 symmetric stretching modes. Other bands are observed in the range 1005–1096 cm^{-1} and are attributed to the ν_3 antisymmetric bending modes of PO_4. Some low intensity bands around 874 cm^{-1} were discovered and remain unclassified. Bands in the low-wavenumber region are assigned to the ν_4 and ν_2 out-of-plane bending modes of the OSiO and PO_4 units. Raman spectroscopy is a useful tool in determining the vibrational spectroscopy of mixed hydrated multi-anion minerals such as perhamite. Information on such a mineral would be difficult to obtain by other means.

Keywords: perhamite, silico-phosphate, Raman spectroscopy, infrared spectroscopy, Tom's phosphate quarry, Moculta phosphate quarry, Penrice marble quarry, Dunton Mine

Introduction

Perhamite is an interesting hydrated silico-phosphate with the formula $Ca_3Al_7(SiO_4)_3(PO_4)_4(OH)_3 \bullet 16.5H_2O$ and was first described from the Bell Pit, Newry, Oxford Co., Maine, USA (Dunn & Appleman, 1977). The presence of phosphate and silicate anions with hydroxyls and water makes perhamite an ideal mineral to study using Raman spectroscopy, as well as infrared and high resolution thermogravimetric analysis (HRTG). This mineral has a questionable crystal structure and Raman spectroscopy may assist in its structural determination.

• Author for correspondence (r.frost@qut.edu.au)

A good starting point is to study the position of the expected bands of the anions and to observe where they occur in aqueous solutions, then to observe the position of the bands resulting from the vibrational spectroscopy of minerals containing the individual anions.

Infrared spectroscopy has proven most useful for the study of phosphate minerals, particularly for phosphate coatings and sprays [1-4]. Raman spectroscopy has been used to a limited extent in the characterisation of mineral species [5, 6], however mixed-anion minerals such as peisleyite have recently been studied . In aqueous systems, Raman spectra of phosphate oxyanions show a symmetric stretching mode (ν_1) at 938 cm^{-1}, the antisymmetric stretching mode (ν_3) at 1017 cm^{-1}, the symmetric bending mode (ν_2) at 420 cm^{-1} and the ν_4 mode at 567 cm^{-1} [7-9]. The vibrational spectra of other phosphate minerals such as pseudomalachite and reichenbachite show shifts in these values. The ν_1 symmetric stretching mode can be observed at 953 cm^{-1}, ν_2 at 422 and 450 cm^{-1}, ν_3 at 1025 and 1096 cm^{-1}, while the ν_4 mode can be observed at 482, 530, 555 and 615 cm^{-1}. Libethenite vibrational modes occur at 960 (ν_1), 445 (ν_2), 1050 (ν_3) and 480, 522, 555, 618 and 637cm^{-1} (ν_4). Cornetite vibrational modes occur at 960 (ν_1), 415 and 464 (ν_2), 1000, 1015 and 1070 (ν_3) and 510, 527, 558, 582, 623 and 647 cm^{-1} (ν_4).

The silicate anion has symmetric stretching modes around 1040 cm^{-1} and bending modes around 420 cm^{-1}. Limited data are available on the variability of these modes in the literature. This work shows that Raman spectroscopy can be readily used to determine phosphate and silicate in minerals, as well as water and hydroxyl units. Raman spectroscopy serves to elucidate the structures of multi-anion minerals.

Occurrence

At the type locality, perhamite forms isolated brown spherulitic masses (about 1mm across) of platy crystals, associated with siderite, wardite, amblygonite, brown eosphorite and sphalerite [10]. The Dunton Mine, also in Newry, was the second occurrence [10], where perhamite formed very soft, delicate, white botryoidal clusters comprised of intergrown platelets (Figure 1). Perhamite has also been discovered in several locations in Maine [11], Nevada [12],Utah and Germany [13]. For a full listing of localities see Mills (2006) [14].

The three Australian occurrences of perhamite originate from quarries exploiting a localised phosphate concentration at the base of the Brighton (Upper Precambrian) limestone [15] in the Kapunda–Angaston area (Figure 2) of the Mt Lofty Ranges, South Australia.

At the three Australian quarries (Toms, Penrice and Moculta) the habits of perhamite include: Crusts and small stalagmite-like aggregates that are made up of platelets less than 0.5 μm thick and range from 5 μm–15 μm wide (Figure 3); intergrown plate-like masses, with individual platelets less than 7 μm in length (Figure 4); and intergrown blades which typically form rosettes, and are generally less than 40 μm across (Figure 5).

Samples from the three Australian occurrences as well as from the Dunton Mine have been used in this vibrational study.

Crystallography

Dunn & Appleman (1977) studied single perhamite crystals from the type locality using a Buerger precession camera. Their results showed that perhamite is a hexagonal mineral with diffraction symmetry 6/mmmP---(P6/***) compatible with space groups $P6_{22}$, $P6_{mm}$, $P6_{m2}$, $P6_{2m}$, $P6_{mmm}$. The crystal structure of perhamite on single crystals from the Smithsonian Institute specimen 143393 has been published [14].

Experimental

Raman microprobe spectroscopy

Samples of perhamite from the Museum Victoria collection (M37630, Toms quarry and M45617, Penrice quarry), CSIRO Minerals collection (MC1254, Moculta quarry) and Smithsonian Institute mineral collection (143393, Dunton Mine) were placed and orientated on the stage of an Olympus BHSM microscope, equipped with 10x and 50x objective lenses, as part of a Renishaw 1000 Raman microscope system. This system also includes a monochromator, filter system and a Charge Coupled Device (CCD). Raman spectra were excited by a HeNe laser (633 nm) at a resolution of 2 cm^{-1} in the range between 100 and 4000 cm^{-1}. Repeated acquisition using the highest magnification was undertaken to improve the signal-to-noise ratio. Spectra were calibrated using the 520.5 cm^{-1} line of a silicon wafer. In order to ensure that the correct spectra were obtained, the incident excitation radiation was scrambled, while spectra at controlled temperatures were obtained using a Linkam thermal stage (Scientific Instruments Ltd, Waterfield, Surrey, England). Previous studies provide an in depth account of the experimental technique [7, 16-20]. Spectral manipulation such as baseline adjustment, smoothing and normalisation was performed using the GRAMS® software package (Galactic Industries Corporation, Salem, NH, USA).

Infrared absorption spectroscopy

Infrared spectra were obtained using a Nicolet Nexus 870 FTIR spectrometer with a smart endurance single bounce diamond ATR cell. Spectra over the 4000–525 cm^{-1} range were obtained by the co-addition of 64 scans with a resolution of 4 cm^{-1} and a mirror velocity of 0.6329 cm/s.

Results and discussion

The spectral region of the SiO_4 and PO_4 stretching vibrations (800–1200 cm^{-1}) was observed for the four mineral samples and their combined spectrum is reported in Figure 6, with the component analyses in Table 1. The Raman spectrum of sample M37630 shows a single band at 1111 cm^{-1}, while the spectrum of M45617 shows two bands at 1122 and 1096 cm^{-1}. The Raman spectra of 143393 (1153 and 1131 cm^{-1})

and MC1254 (1110 and 1185 cm^{-1}) show slight shifts in these values. The bands in this region are attributed to the stretching vibration of SiO_4. In the infrared spectrum, bands are observed at 1110, 1185 and 1218 cm^{-1} (M37630) and 1144, 1186, 1215 and 1311 cm^{-1} (M45617). Identical bands are present in the IR spectrum of all samples, however, M45617 has an additional band. These four bands are attributed to SiO_4 stretching vibrations.

In the Raman spectra, an intense band is observed at around 988 cm^{-1} in sample M37630. An equivalent band of lesser intensity is found in the infrared spectrum at 976 and 993 cm^{-1}. The same band is observed in sample 143393 at 996 cm^{-1}, and at 966 cm^{-1} for sample MC1254. These bands are assigned to the ν_1 symmetric stretching mode of the PO_4 units. Two bands are observed at 1009 and 1039 cm^{-1} (M37630), 1012 and 1039 cm^{-1} (M45617), and at 1076 and 1041 cm^{-1} for MC1254 and can be attributed to the ν_3 PO_4 antisymmetric stretching modes. In sample 143393 two extra bands are observed (1096, 1059, 1032 and 1005 cm^{-1}). The observation of additional bands for sample 143393 provides an indication of the symmetry reduction of the PO_4 units for this mineral. In the infrared spectra the equivalent bands are observed at the higher wavenumbers 1020 and 1055 cm^{-1} for M37630 and at 1019, 1049 and 1054 cm^{-1} for M45617. The intensity of these bands is greater in the infrared spectrum. The symmetrical stretching modes show much greater intensity in the Raman spectrum, whilst the infrared spectrum shows much higher intensity for the asymmetric stretching modes. Raman spectroscopy complemented with infrared spectroscopy enables the assignation of bands to the SiO_4 and PO_4 stretching vibrations. The advantage of Raman spectroscopy rests with the capacity for band separation.

It should also be noted that the amount of material of sample 143393 was insufficient to obtain an infrared spectrum. Raman microscopy has the major advantage of analysing very small amounts of material of the order of 1 μm size. It is noteworthy that a low intensity band is observed around 874 cm^{-1}. This band is not observed in the Raman spectra and is attributed to the water librational modes.

The Raman and infrared spectra of the low wavenumber region of perhamite are shown in Figure 7. The infrared spectral limit is 550 cm^{-1}. Bands below this wavenumber are not observed in the infrared spectrum using the techniques employed in this research. One of the major advantages of Raman spectroscopy is the ability to obtain spectra in the low wavenumber region with minimal sample preparation other than the alignment of the crystals relative to the incident radiation. Bands in this spectral region are assignable to the bending modes of the SiO_4 and PO_4 units. An intense band is observed in the infrared spectrum at 588 cm^{-1}. The equivalent band in the Raman spectrum is at around 580 cm^{-1}. The band is observed at 586 cm^{-1} for sample 143393 and 582 cm^{-1} for sample MC1254. These bands are attributed to the ν_4 out of plane bending modes of the PO_4 units. It is noted that an additional band is observed for the ν_4 bending mode at 554 for sample 143393 and provides a further indication of symmetry lowering of the PO_4 units for this mineral. An intense band is observed in the Raman spectrum at around 470 cm^{-1}. This band is attributed to the ν_2 PO_4 bending mode. Two other bands are observed at 376 and 402 cm^{-1}. These bands are ascribed to the OSiO bending modes. Two bands are observed at around 518 and 532 cm^{-1} and may be assigned to OH deformation modes. Two intense bands are

observed at around 196 and 272 cm^{-1}. These bands are assigned to CaO and Al_2O_3 stretching vibrations.

The infrared spectrum of sample M37630 shows a number of overlapping bands in the hydroxyl stretching region. Bands are observed at 3581, 3489, 3371, 3311 and 3078 cm^{-1}. Studies have shown a strong correlation between OH stretching frequencies and both O···O bond distances and H···O hydrogen bond distances [21-24]. Libowitzky (1999) showed that a regression function can be employed relating the hydroxyl stretching frequencies with regression coefficients better than 0.96 using infrared spectroscopy [25]. The function is described as: $\nu_1 = (3592 - 304) \times 109^{\frac{-d(O-O)}{0.1321}}$ cm^{-1}. Thus OH---O hydrogen bond distances may be calculated using the Libowitzky empirical function. The values for the OH stretching vibrations listed above provide hydrogen bond distances of 3.176(0) Å (3581 cm^{-1}), 2.880(5) Å (3489 cm^{-1}), 2.779(6) Å (3371 cm^{-1}), 2.749(3) Å (3311 cm^{-1}), 2.668(1) Å (3078 cm^{-1}) and 2.599(7) Å (2729 cm^{-1}). The large hydrogen bond distances (Figure 8) which are present in perhamite can also be seen in other mixed anion minerals such as peisleyite (Frost *et al.,* in press[a]) where the distances ranging between 3.052(5) and 2.683(6) Å. Such hydrogen bond distances are typical of secondary minerals. A range of hydrogen bond distances are observed from reasonably strong to weak hydrogen bonding. This range of hydrogen bonding contributes to the stability of the mineral.

Two types of OH units can be identified in the structure of perhamite (Figure 9). The hydrogen bond distances previously established can be used to predict the hydroxyl stretching frequencies. The spectrum of peisleyite may be divided into two groups of OH stretching wavenumbers; namely 3300–3700 cm^{-1} and 2900–3300 cm^{-1}. This distinction suggests that the strength of the hydrogen bonds as measured by the hydrogen bond distances can also be divided into two groups according to the H-bond distances. An arbitrary cut-off point may be 2.74 Å based upon the wavenumber 3300 cm^{-1}. Thus the first four bands listed above may be described as weak hydrogen bonds and the last two bands as relatively strong hydrogen bonds. The infrared spectra of the second perhamite sample gave bands in similar positions to the first sample and hydrogen bond distances are identical. It should be noted that a quite intense band at 1671 cm^{-1} is assigned to the water HOH bending mode. For normal hydrogen-bonded water this band occurs at around 1630 cm^{-1}. Thus the position of the band also indicates strong hydrogen bonding in the mineral.

Conclusions

Mixed hydrated multi-anion minerals such as perhamite are ideal for this application and their characterisation enables a wider understanding of both common anion positions (e.g. PO_4, SO_4, AsO_4 and SiO_4) and variances in hydrogen bond lengths. This technique also has the advantages of obtaining the spectra of the minerals with no sample preparation; the minerals can be measured *in situ* on the host matrix; and spectra below 400 cm^{-1} can be readily measured.

Estimates of the hydrogen-bond distances have been made from the position of the OH stretching vibrations and show a wide range in both strong and weak bonds.

These ranges are not dissimilar to other mixed-anion minerals such as peisleyite. Bands attributable to the presence of SiO_4 and PO_4 have also been reported. The data from the four separate localities show that perhamite has consistent spectra, enabling positive identification of future occurrences.

Acknowledgements

The financial and infrastructure support of the Queensland University of Technology Inorganic Materials Research Program of the School of Physical and Chemical Sciences is gratefully acknowledged. The Australian Research Council (ARC) is thanked for funding. Museum Victoria, CSIRO Minerals and the Smithsonian Institute are thanked for the loan of the minerals. SJM wishes to thank the support of CSIRO Minerals.

References

[1]. S. Crisp, I. K. O'Neill, H. J. Prosser, B. Stuart and A. D. Wilson, Journal of Dental Research 57 (1978) 245.
[2]. S. V. Gevork'yan and A. S. Povarennykh, Mineralogicheskii Zhurnal 2 (1980) 29.
[3]. S. V. Gevork'yan and A. S. Povarennykh, Konstitutsiya i Svoistva Mineralov 9 (1975) 73.
[4]. C. Paluszkiewicz, A. Stoch, A. Brozek and E. Dlugon, Journal of Molecular Structure 293 (1993) 291.
[5]. N. Satoh, Hyomen Gijutsu 40 (1989) 933.
[6]. M. J. Castagnola and P. K. Dutta, Microporous and Mesoporous Materials 42 (2001) 235.
[7]. R. L. Frost, W. Martens, P. A. Williams and J. T. Kloprogge, Mineralogical Magazine 66 (2002) 1063.
[8]. R. L. Frost, W. N. Martens, T. Kloprogge and P. A. Williams, Neues Jahrbuch fuer Mineralogie, Monatshefte (2002) 481.
[9]. R. L. Frost, P. A. Williams, W. Martens, J. T. Kloprogge and P. Leverett, Journal of Raman Spectroscopy 33 (2002) 260.
[10]. P. J. Dunn and D. E. Appleman, Mineralogical Magazine 41 (1977) 437.
[11]. V. T. King, *Selected history of Maine mining and minerals., Vol. Mineralogy of Maine, Volume 2*, Maine Geological Survey, Maine, USA, 2000.
[12]. S. Pullman and R. Thomssen, Nevada Mineral Locality Index 74 (1999) 370.
[13]. G. Blab and H. W. Graf, Mineralien-Welt 6 (1995) 26.
[14]. S. Mills, G. Mumme, I. Grey and P. Bordet, Mineralogical Magazine 70 (2006) 201.
[15]. E. S. Pilkington, E. R. Segnit and J. A. Watts, Mineralogical Magazine 46 (1982) 449.
[16]. R. L. Frost, M. Crane, P. A. Williams and J. T. Kloprogge, Journal of Raman Spectroscopy 34 (2003) 214.
[17]. R. L. Frost, P. A. Williams and W. Martens, Mineralogical Magazine 67 (2003) 103.
[18]. W. Martens, R. L. Frost and J. T. Kloprogge, Journal of Raman Spectroscopy 34 (2003) 90.
[19]. W. Martens, R. L. Frost, J. T. Kloprogge and P. A. Williams, Journal of Raman Spectroscopy 34 (2003) 145.
[20]. R. L. Frost, W. Martens, J. T. Kloprogge and P. A. Williams, Journal of Raman Spectroscopy 33 (2002) 801.
[21]. J. Emsley, Chemical Society Reviews 9 (1980) 91.
[22]. H. Lutz, Structure and Bonding (Berlin, Germany) 82 (1995) 85.
[23]. W. Mikenda, Journal of Molecular Structure 147 (1986) 1.
[24]. A. Novak, Structure and Bonding (Berlin) 18 (1974) 177.
[25]. E. Libowitsky, Monatschefte fÜr chemie 130 (1999) 1047.

Raman								IR			
M37630		**M45617**		**143393**		**MC1254**		**M37630**		**M45617**	
Centre (cm^{-1})	Area	Centre (cm^{-1})	Area	Centre (cm^{-1})	Area	Centre (cm^{-1})	Area	Centre (cm^{-1})	Area	Centre (cm^{-1})	Area
								3581	0.024	**3585**	0.033
								3489	0.079	**3483**	0.164
								3371	0.229		
								3311	0.003	**3326**	0.291
										3179	0.020
								3078	0.628	**3065**	0.460
										2922	0.000
										2853	0.001
										2783	0.028
								2729	0.036		
										2618	0.004
				1884	0.031	**1883**	0.025				
								1656	0.032	**1671**	0.009
										1635	0.052
								1610	0.028		
								1483	0.032	**1483**	0.049
1446	0.010	**1440**	0.046					**1438**	0.034	**1429**	0.018
1342	0.034	**1337**	0.005	**1354**	0.022	**1352**	0.012				
								1321	0.004	**1311**	0.001
				1245	0.029	**1241**	0.034				

								1218	0.023	**1215**	0.019
								1185	0.008	**1186**	0.003
				1153	0.015	**1151**	0.033			**1144**	0.064
				1131	0.018	**1127**	0.017				
1111	0.066	**1122**	0.028					**1110**	0.180		
		1096	0.062	**1096**	0.015						
		1080	0.001			**1076**	0.081				
				1059	0.010			**1055**	0.152	**1054**	0.327
										1049	0.005
1039	0.185	**1039**	0.136			**1041**	0.074				
				1032	0.157						
								1020	0.178	**1019**	0.064
1009	0.037	**1012**	0.029	**1005**	0.074						
988	0.140	**989**	0.252	**996**	0.072					**993**	0.229
		941	0.033					**976**	0.120		
						966	0.286				
						962	0.129			**956**	0.022
				929	0.007						
								874	0.021	**879**	0.015
		805	0.006								
										751	0.003
708	0.014	**712**	0.006	**708**	0.051						
		628	0.001	**636**	0.019						
621	0.083	**623**	0.084	**615**	0.051	**618**	0.008				
						608	0.022				

						593	0.012	**588**	0.191	**588**	0.055
582	0.052	**580**	0.041	**586**	0.009	**582**	0.035				
				554	0.021						
532	0.012	**523**	0.012	**520**	0.072						
518	0.038	**514**	0.037								
				506	0.100						
470	0.034	**473**	0.034	**468**	0.030						
				442	0.007	**451**	0.048				
421	0.003					**433**	0.050				
402	0.029	**399**	0.008								
				385	0.013						
376	0.052	**373**	0.036	**375**	0.050						
				363	0.009						
				334	0.014						
						305	0.017				
272	0.062	**273**	0.088	**276**	0.034	**274**	0.055				
				267	0.016						
				207	0.020	**208**	0.015				
196	0.047	**196**	0.039	**191**	0.021						
168	0.002	**176**	0.004	**170**	0.004	**171**	0.007				
150	0.019	**151**	0.003			**153**	0.002				
		145	0.001	**148**	0.003	**147**	0.016				
132	0.010	**132**	0.002	**129**	0.004	**130**	0.014				
115	0.000	**114**	0.000								

Table 1

List of Figures

List of Tables

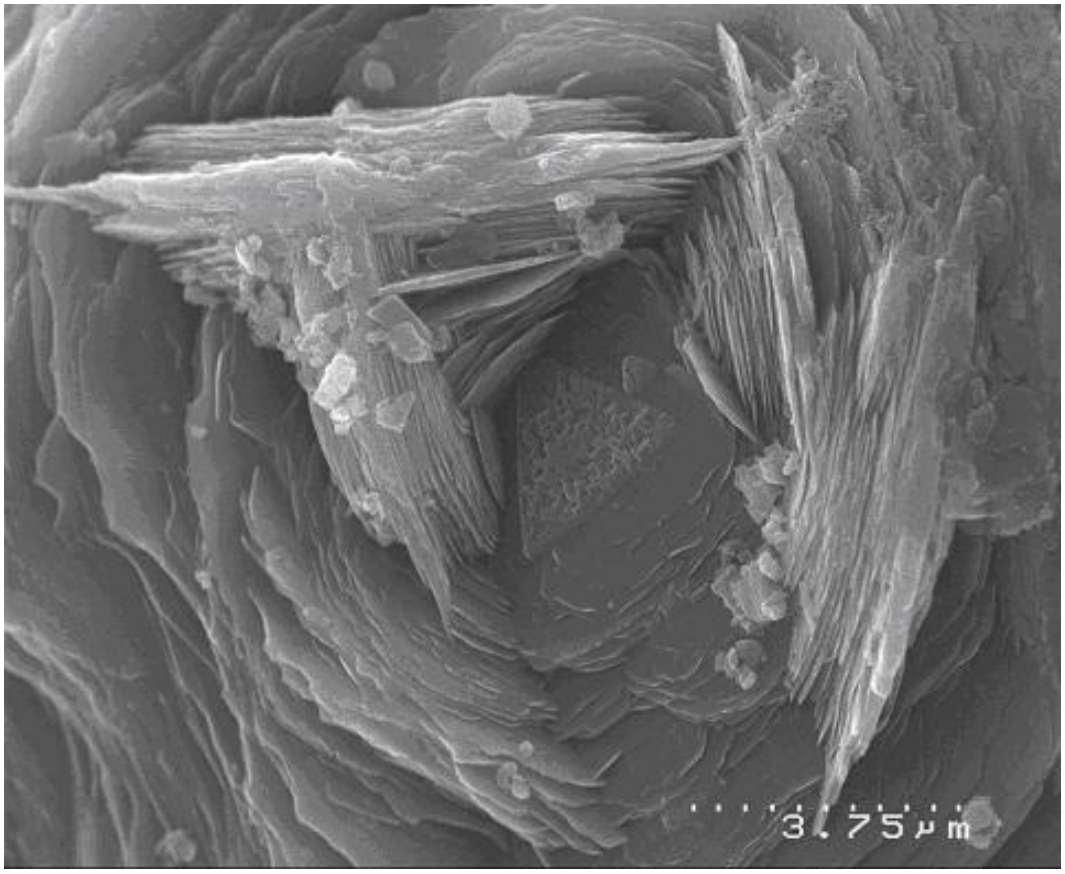

Figure 1.

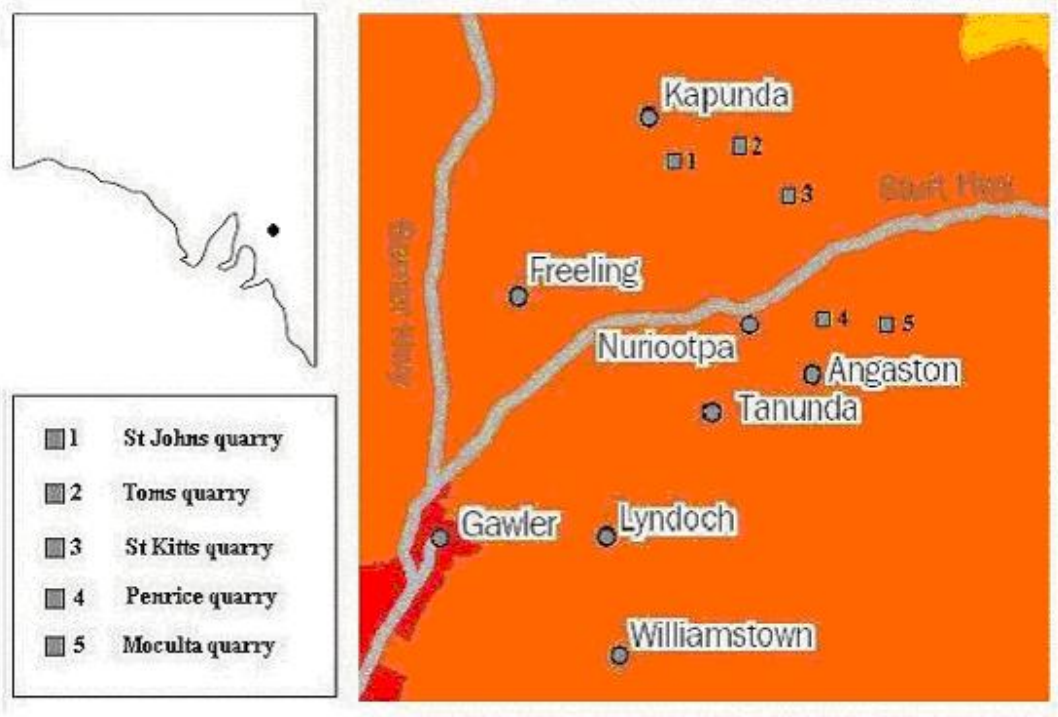

Figure 2.

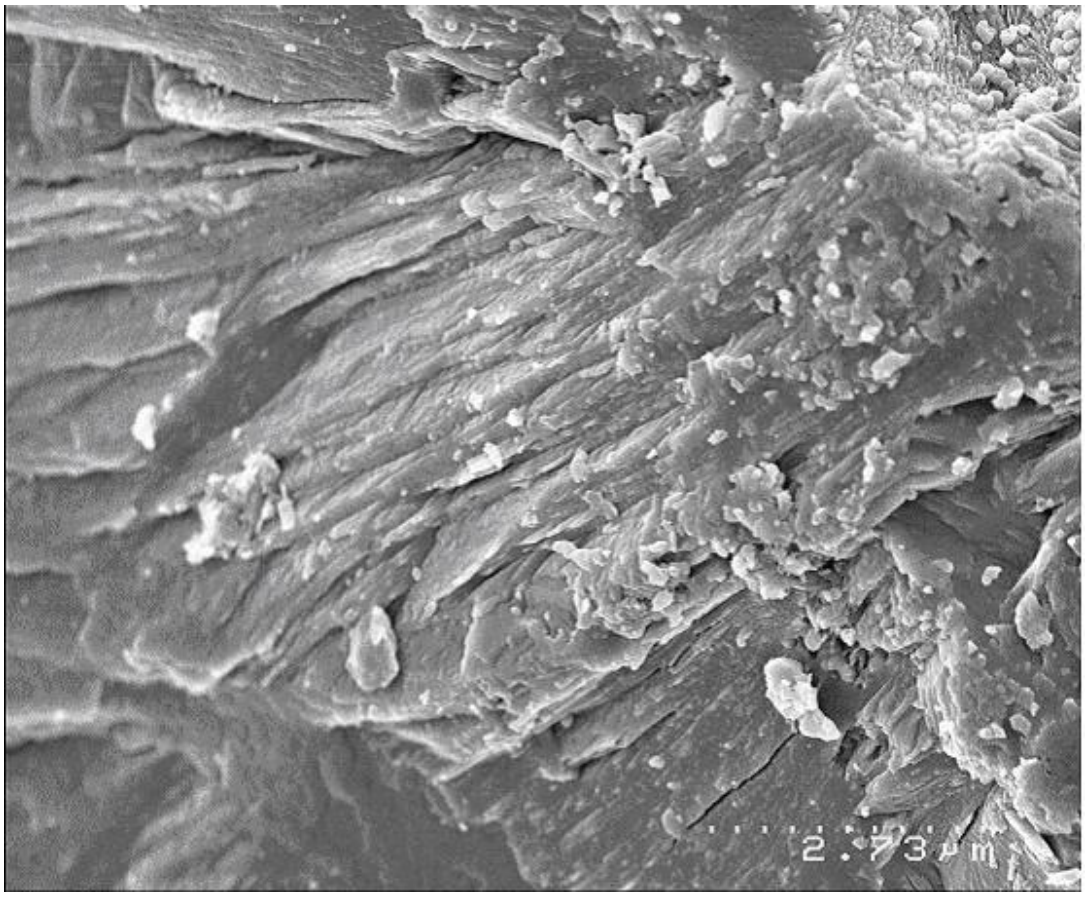

Figure 3

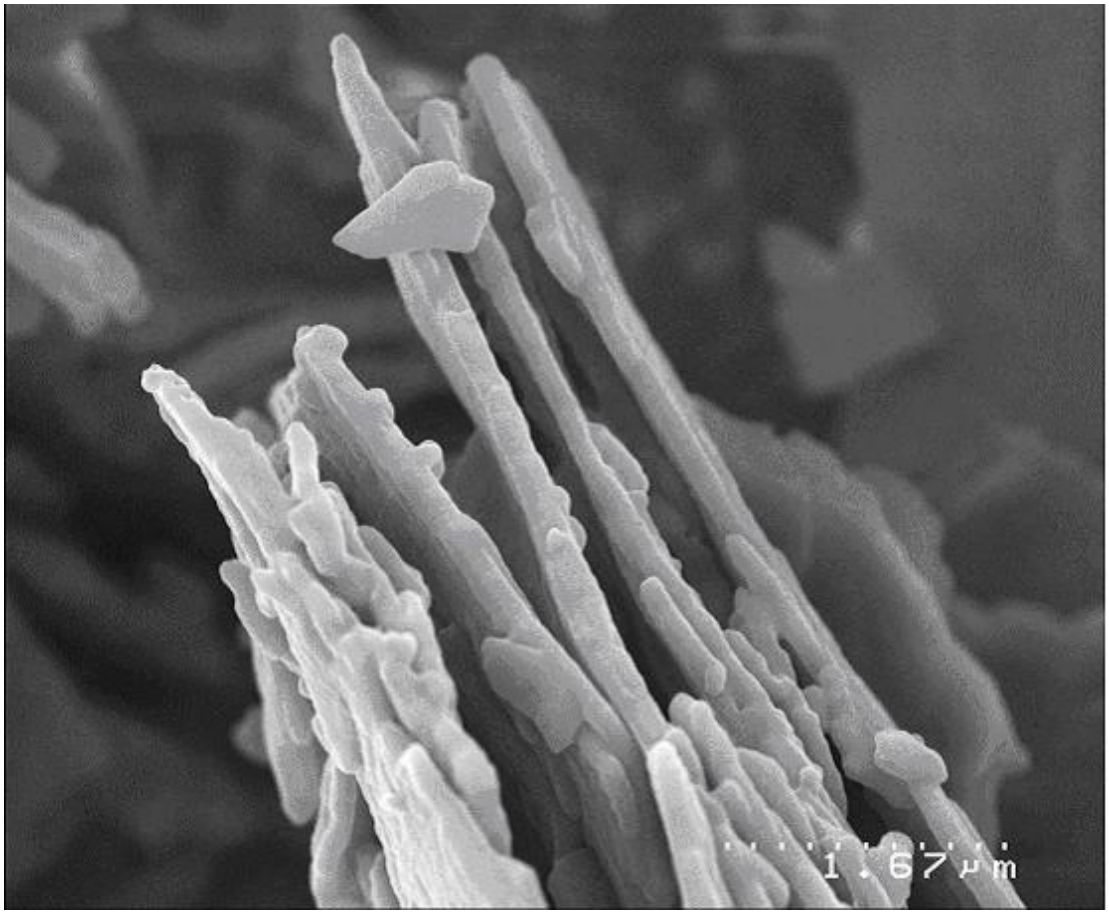

Figure 4.

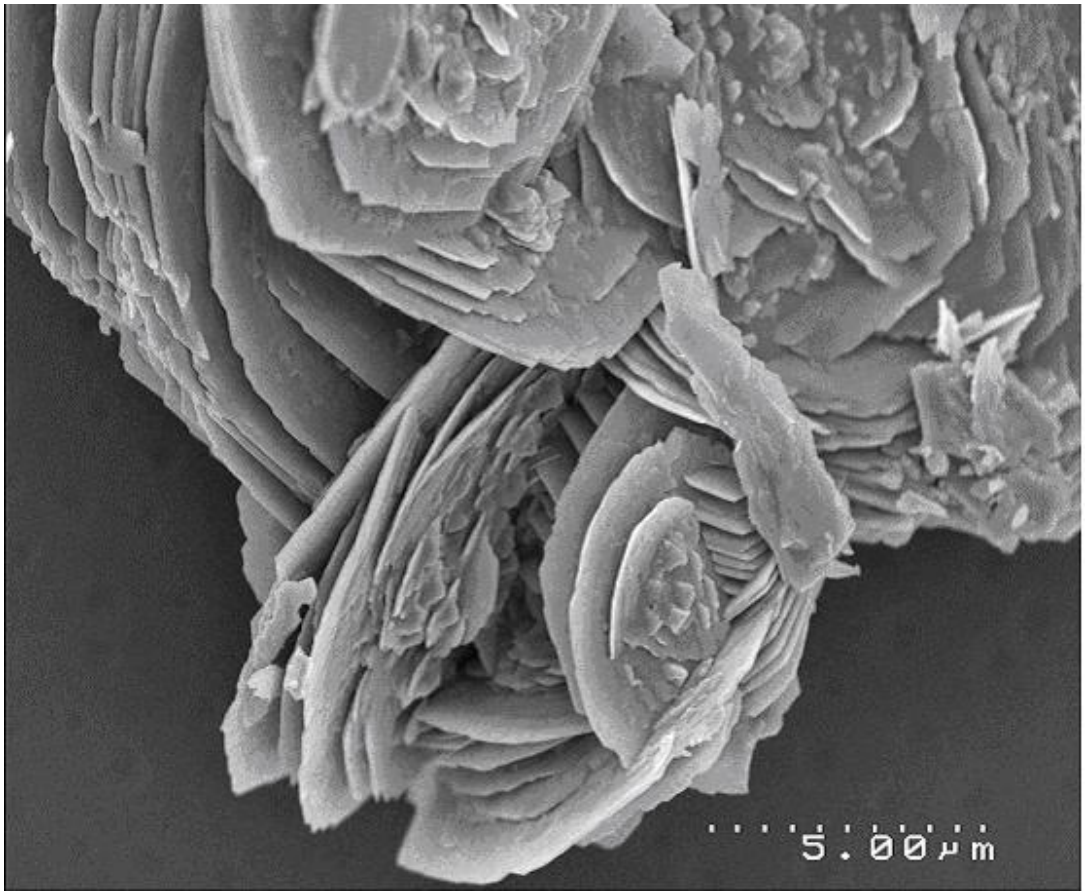

Figure 5

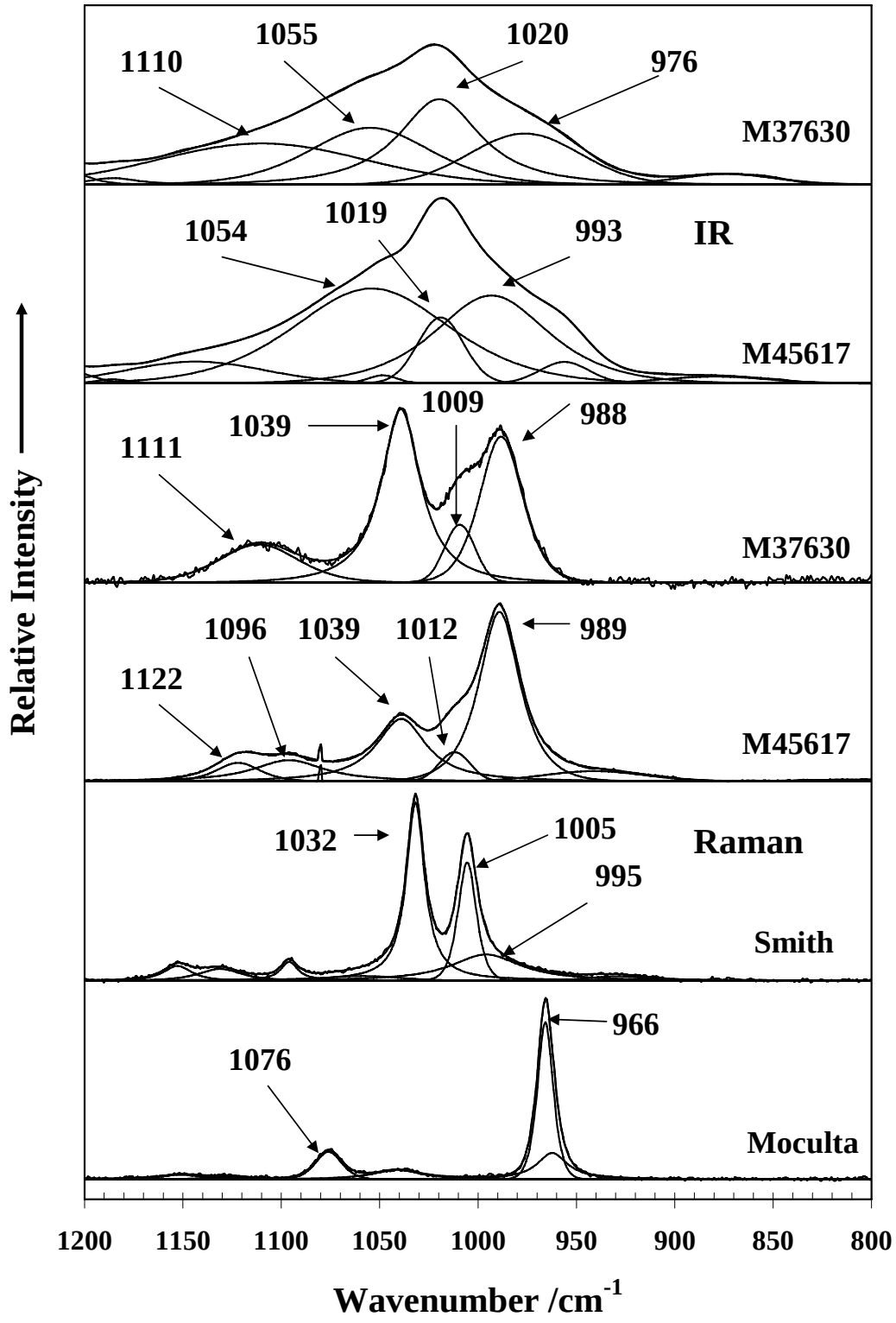
1110
1055
1020
976
M37630
1054
1019
993
IR
M45617
1111
1039
1009
988
M37630
1122
1096
1039
1012
989
M45617
1032
1005
995
Raman
Smith
1076
966
Moculta
Relative Intensity
1200
1150
1100
1050
1000
950
900
850
800
Wavenumber /cm-1

Figure 6.

Figure 7

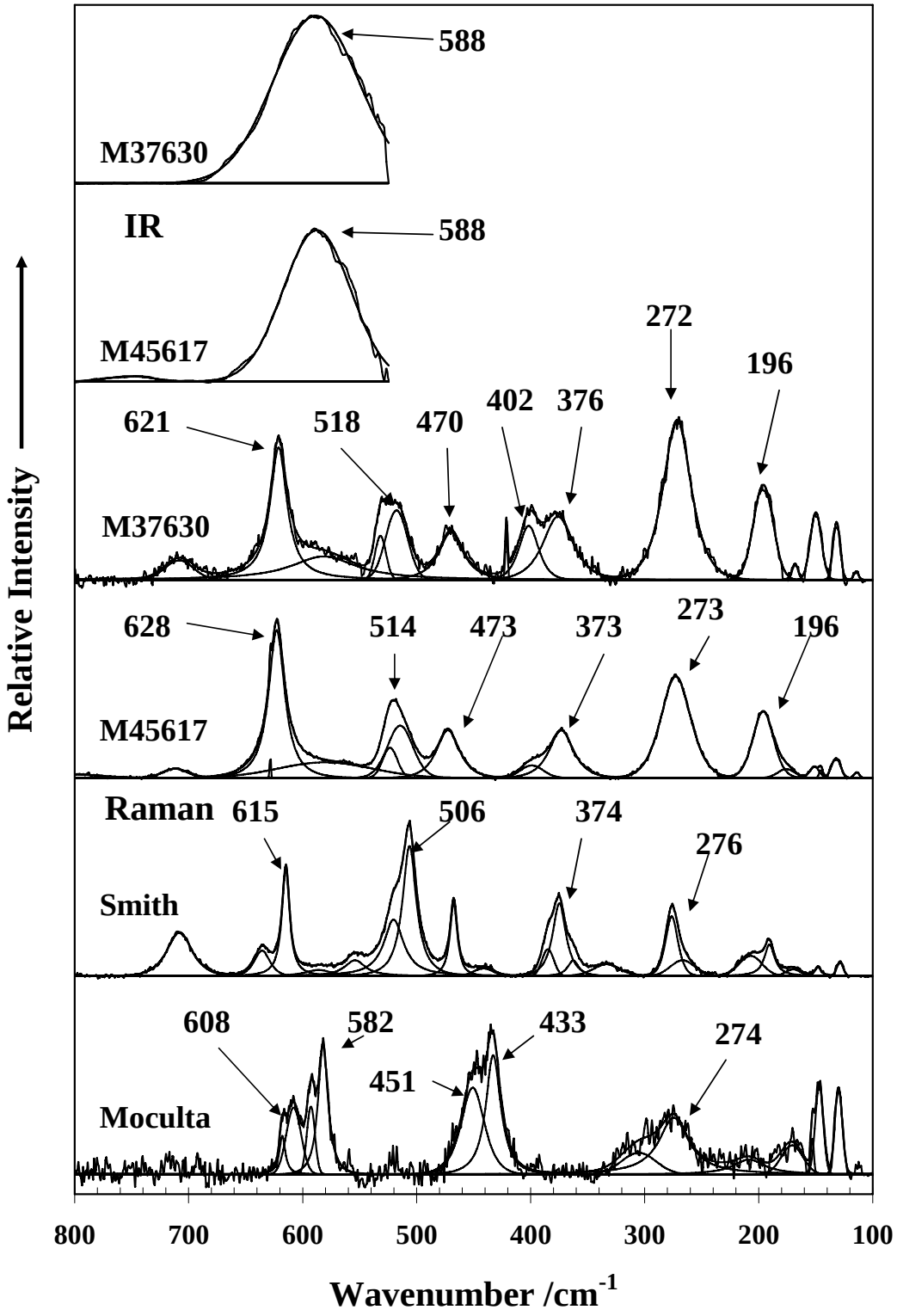
588
M37630
IR
588
M45617
272
196
621
518
470
402
376
M37630
628
514
473
373
273
196
M45617
Raman
615
506
374
276
Smith
608
582
433
274
451
Moculta
Relative Intensity
800
700
600
500
400
300
200
100
Wavenumber /cm-1

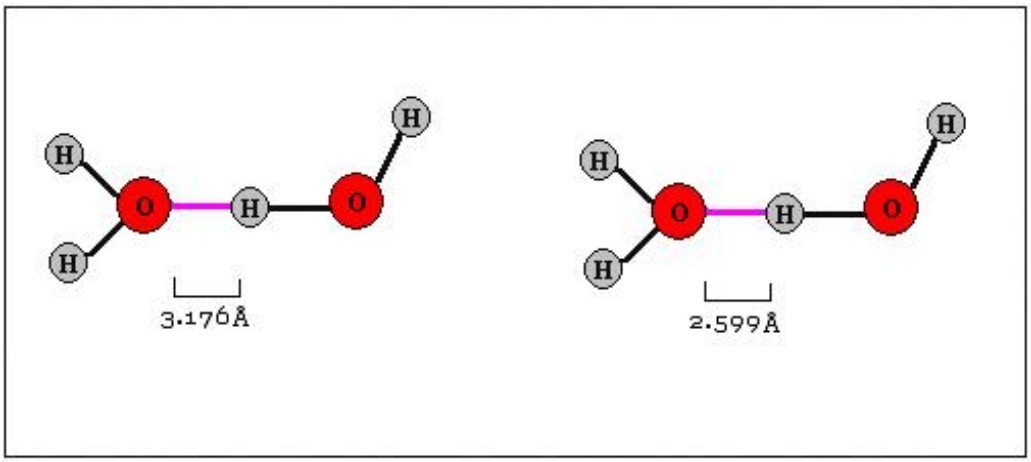

Figure 8

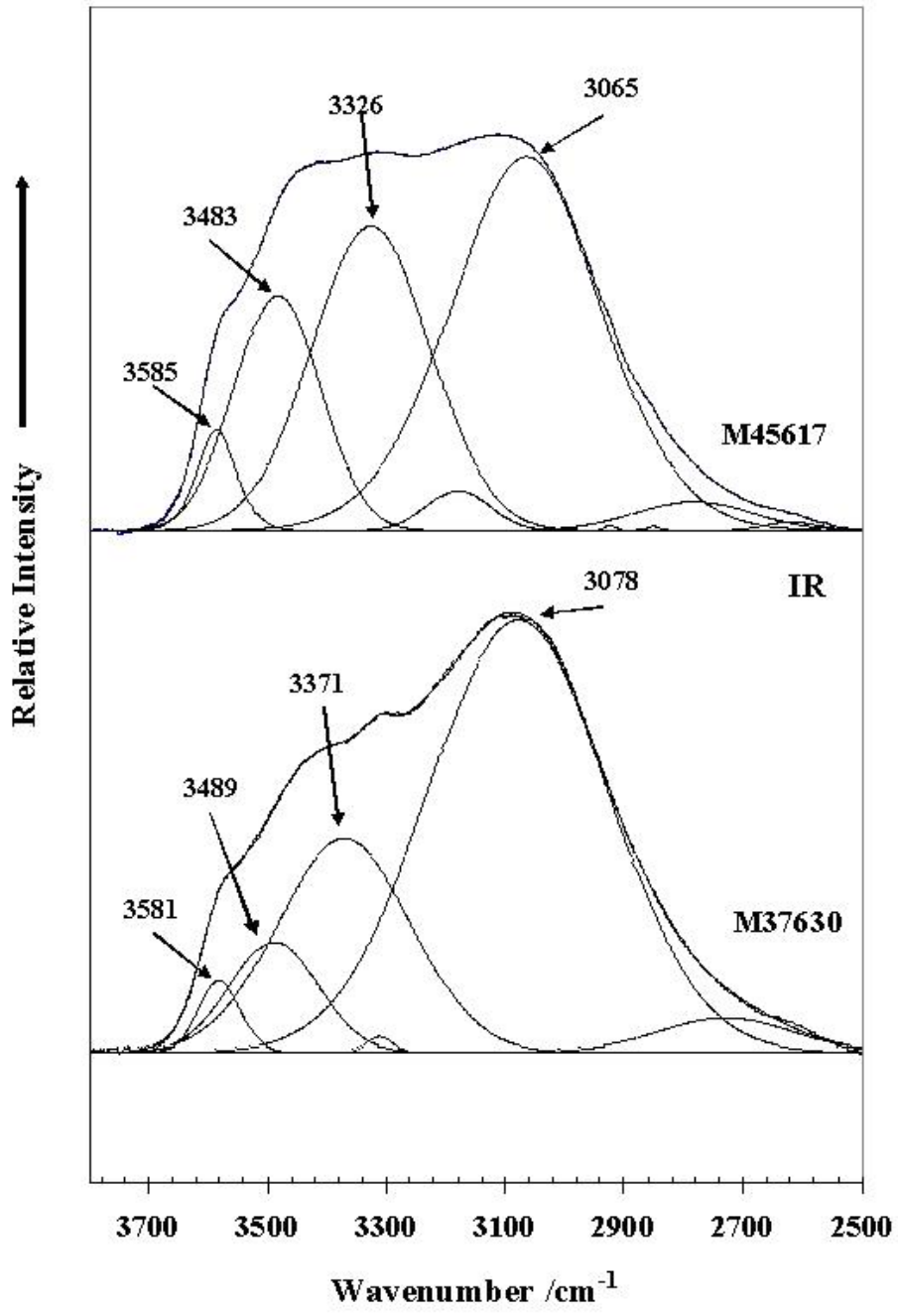
3326
3065
3483
3585
M45617
IR
3078
3371
3489
3581
M37630
Relative Intensity
3700
3500
3300
3100
2900
2700
2500
Wavenumber /cm-1

Figure 9